condensed matter

MDPI

Article

Dynamic Correlations in Disordered Systems: Implications for High-Temperature Superconductivity

Takeshi Egami [1,2]

[1] Shull-Wollan Center, Department of Materials Science and Engineering, Department of Physics and Astronomy, University of Tennessee, Knoxville, TN 37996, USA; egami@utk.edu
[2] Materials Sciences and Technology Division, Oak Ridge National Laboratory, Oak Ridge, TN 37831, USA

Abstract: Liquids and gases are distinct in their extent of dynamic atomic correlations; in gases, atoms are almost uncorrelated, whereas they are strongly correlated in liquids. This distinction applies also to electronic systems. Fermi liquids are actually gas-like, whereas strongly correlated electrons are liquid-like. Doped Mott insulators share characteristics with supercooled liquids. Such distinctions have important implications for superconductivity. We discuss the nature of dynamic atomic correlations in liquids and a possible effect of strong electron correlations and Bose–Einstein condensation on the high-temperature superconductivity of the cuprates.

Keywords: superconductivity; liquid and glass; dynamic correlation; disorder

check for updates

Citation: Egami, T. Dynamic Correlations in Disordered Systems: Implications for High-Temperature Superconductivity. *Condens. Matter* **2024**, *9*, 12. https://doi.org/10.3390/condmat9010012

Academic Editor: Andrzej M. Oleś

Received: 20 December 2023
Revised: 29 January 2024
Accepted: 31 January 2024
Published: 3 February 2024

1. Introduction

At ambient pressure, liquid evaporates to gas through a first-order phase transition. So, the common perception is that liquids and gases represent different phases of matter. However, the distinction between liquids and gases is not as obvious as it may appear. For instance, liquid changes into gas continuously under high pressure beyond the tri-critical point [1]. From a more fundamental point of view, the crucial difference between gases and liquids is in the way that the interatomic potential, $V(r)$, affects the dynamics [2–4]. In an ideal gas, atoms interact with each other only through occasional collisions, so that the average potential energy, $<U>$, is practically zero. This happens at a low density, or equivalently, at a high temperature where the effective atomic radius, R_{eff}, defined by $V(2R_{eff}) = k_BT$, is much smaller than the radius determined by the minimum in $V(r)$. On the other hand, atoms in a liquid are always influencing each other through the interatomic potential, so $<U>$ is non-zero and plays a major role in the dynamics.

The distinction between liquids and gases can be found most clearly in the specific heat, C_V. In an ideal gas, $C_V = (3/2)k_B$, whereas in liquid, $C_V = 3\,k_B$ [5,6]. This is because in gas, $<U> \cong 0$, so that the specific heat originates only from the kinetic energy, $<T> = (3/2)k_BT$. In contrast, atoms in a liquid are always influencing each other through the interatomic potential. Thus, through the equipartition theorem, $<U> = <T>$, resulting in $C_V = 3k_B$, known as Dulong–Petit law for solids [7]. In other words, liquid is condensed matter, not a high-density gas. Indeed, the physical density of a liquid is almost as high as that of a solid [8]. In gas, atom–atom interactions are collisional. In liquid, atoms are held together by cohesive forces, just as in a solid, and atomic motions are vibrational [9].

However, it is quite challenging to formulate theories of such strongly and randomly interacting atoms. In crystals, the lattice periodicity greatly simplifies our understanding, and the theories of condensed matter physics are well established [7]. In contrast, to study liquids, we have to face the dynamic many-body problem directly. For this reason, the progress in the science of liquids has been slow, despite a large amount of effort over many years [2–4,10–43]. In the absence of an obvious starting point, many early ideas and theories of liquids were based upon the models of high-density gases, in spite of the important

differences between liquids and gases. For instance, the hard-sphere (HS) model [12–14] is a gas model with $<U> = 0$. Widely used concepts, such as free-volume [15–17] and jamming [37,38], stem from the HS model, and thus, they assume that a liquid is basically a high-density gas. The Weeks–Chandler–Andersen principle [43] states that at high temperatures, only the repulsive part of the potential is relevant, thus the HS model is always justified. Here, the role of the potential is essentially neglected. However, as we discuss below, the potential energy plays a critical role in controlling the properties of a liquid, supercooled liquid in particular.

Because there are fundamental and qualitative differences between the gas model and the liquid/solid model, we believe that it is better to start with an elastic model in which the harmonic interaction is assumed from the beginning, instead of starting with the gas model and increasing the density to describe a liquid. Such an approach, based on the concept of atomic-level stresses [44] and the density wave instability [45], had major success in describing the evolution of the structure of a liquid with temperature [46] and in elucidating the glass transition [47]. In this paper, we briefly describe this theory and discuss the atomic dynamics in superfluid ^{4}He observed by inelastic neutron scattering [48] and the possible implication of this observation on the mechanism of the high-temperature superconductivity of the cuprates [49].

2. Local Structure of Liquid and Glass

In 1952, Frank [50] suggested that icosahedral clusters of atoms (Figure 1) may exist in a liquid to explain the high degree of supercooling observed by Turnbull [51]. He argued that for the Lennard–Jones potential, an icosahedral cluster has an 8.4% lower energy than the close-packed *f.c.c.* cluster. Icosahedral clusters cannot be the basis of a simple crystalline phase because of the predominant five-fold symmetry, whereas it can exist as a short-range order (SRO) in an aperiodic structure of a liquid. Frank argued that for this reason, crystallization from a liquid requires significant structural reorganization, and this presents the energy barrier for the transformation from a liquid to a crystal, resulting in supercooling [50]. Soon, Bernal discovered a high density of icosahedral clusters in his random-packed HS model [12,13]. Since then, the idea of regarding the icosahedral cluster or similar high-symmetry clusters as the building block to form a glass structure became the standard approach in the effort to elucidate the structure of metallic glass [52–58].

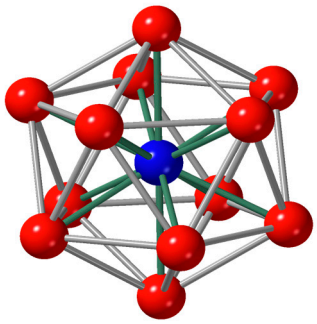

Figure 1. An icosahedral cluster.

The structure of liquid and glass is usually expressed in terms of the atomic pair-distribution function (PDF), $g(r)$, given by

$$g(r) = \frac{1}{N}\sum_{i,j}\delta\left(r - \left|\boldsymbol{r_i} - \boldsymbol{r_j}\right|\right) \quad (1)$$

where $\boldsymbol{r_i}$ is the position of the i-th atom, and N is the total number of atoms, or $G(r) = 4\pi r\rho_0[g(r) - 1]$, where ρ_0 is the atomic number density [2–4]. The PDF describes only the two-body correlation, whereas the full description of the real structure requires high-order correlations as well [2–4]. However, because the PDF can be directly determined

by a diffraction experiment with X-ray or neutrons [59], it is an excellent starting point. Also, even though it is a two-body correlation function, its features reflect higher-order correlations. For instance, its n-th order derivative with r contains information on the correlations among $2 + n$ particles. In particular, the oscillations in the PDF beyond the first peak describe the medium-range order (MRO) in the coarse-grained density fluctuations, rather than the detailed position of each atom [60], as discussed below.

In 1914, Ornstein and Zernike (OZ) [10] proposed a scheme to connect the SRO and the MRO through a mean-field convolution equation. They divide the PDF into two parts,

$$g(\boldsymbol{r}) = 1 + c(\boldsymbol{r}) + h(\boldsymbol{r}), \tag{2}$$

where $c(\boldsymbol{r})$ describes the short-range correlation, and $h(\boldsymbol{r})$ is the medium-range correlation. Beyond the first peak, $c(\boldsymbol{r}) = 0$. The $c(\boldsymbol{r})$ is directly influenced by the interatomic potential. Then, they propose a mean-field convolution equation,

$$h(\boldsymbol{r}) = c(\boldsymbol{r}) + \rho_0 \int c(|\boldsymbol{r} - \boldsymbol{r}'|) h(\boldsymbol{r}') d\boldsymbol{r}'. \tag{3}$$

Its Fourier-transform to the structure function

$$S(\boldsymbol{Q}) = 1 + c(\boldsymbol{Q}) + h(\boldsymbol{Q}), \tag{4}$$

$$h(\boldsymbol{Q}) = c(\boldsymbol{Q}) + \rho_0 c(\boldsymbol{Q}) h(\boldsymbol{Q}), h(\boldsymbol{Q}) = \frac{c(\boldsymbol{Q})}{1 - \rho_0 c(\boldsymbol{Q})} \tag{5}$$

shows that the MRO is a direct consequence of the SRO. For instance, the first peak of $c(\boldsymbol{Q})$ directly results in the first peak of $h(\boldsymbol{Q})$ in the amplified manner. Even though it is a 100 year-old theory, the OZ theory is still widely used. However, as shown below, the SRO and the MRO are fundamentally different, with different origins and behaviors. The OZ theory may work for strongly disordered complex soft-matter [61], but it does not work well for supercooled metallic liquids in which atoms are dynamically correlated.

The $S(Q)$ and $g(r)$ are connected by [59]

$$g(r) = \frac{1}{2\pi^2 r \rho_0} \int [S(Q) - 1] sin(Qr) Q dQ. \tag{6}$$

Therefore, a sharp peak in $S(Q)$ results in an oscillating function in $g(r)$, and vice versa. The widely used practice of the one-to-one correspondence between the first peak in $S(Q)$ at Q_1 and the first peak in $g(r)$ at r_1 by $r_1 = 2\pi/Q_1$ [62] does not work. Actually, as shown by Cargill long ago [63], the first peak of $S(Q)$ describes the MRO as shown in Figure 2 [64]. Similarly, the first peak of $g(r)$ that describes the SRO corresponds to the high-Q part of $S(Q)$.

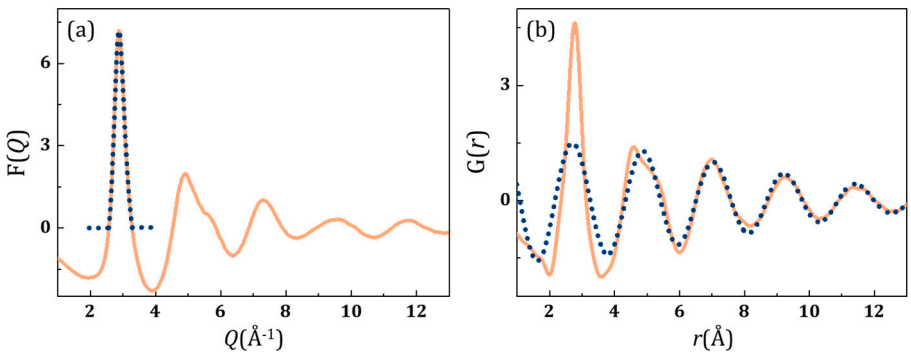

Figure 2. (**a**) $F(Q) = Q[S(Q) - 1]$ for $Pd_{43}Cu_{27}Ni_{10}P_{20}$ glass at T_g = 573 K (solid curve) and the first peak (dotted curve). (**b**) The PDF (solid curve), and the Fourier-transformed first peak of $S(Q)$ (dotted curve) showing that the first peak of $S(Q)$ largely accounts for the MRO oscillations [64].

3. Density Wave Theory of Medium-Range Order

The PDF of metallic liquids and glasses shows prominent exponentially decaying oscillations around the average density with a well-defined periodicity (Figure 3 [65]). The structural coherence length, ξ_s, defined by the exponential decay of $G(r)$,

$$G(r) = G_0(r)exp(-r/\xi_s), \tag{7}$$

obeys the Curie–Weiss law in its temperature dependence [46,65],

$$\xi_s(T) = \frac{C}{T - T_{IG}}. \tag{8}$$

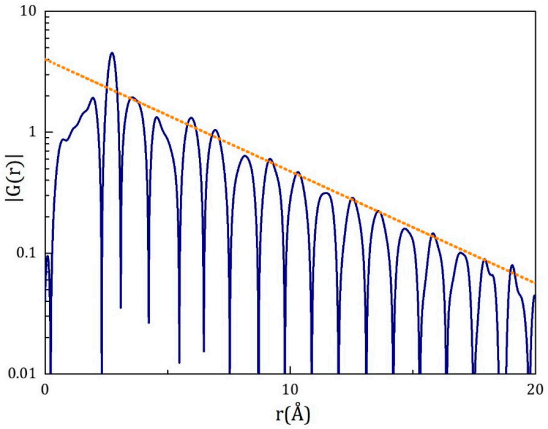

Figure 3. The $|G(r)|$ (in log-scale) of $Pd_{42.5}Ni_{7.5}Cu_{30}P_{20}$ liquid at T = 600 K, just above T_g [65]. The dashed line is a guide to the eye indicating exponential decay.

Equation (8) diverges at T_{IG}; although, it never happens because $T_{IG} < 0$. The state reached by the extrapolation to T_{IG} is characterized by the long-range density wave (DW) correlation [60,65]. This divergence suggests that there is a driving force toward this state, the DW state. The right theoretical framework to study this state is the density wave theory, in which the atomic density, $\rho(\boldsymbol{r})$, is given by

$$\rho(\boldsymbol{r}) = \int \rho(\boldsymbol{q}) e^{i\boldsymbol{q}\cdot\boldsymbol{r}} d\boldsymbol{q}. \tag{9}$$

The Fourier-transform of the interatomic potential, $\phi(\boldsymbol{q})$, is dominated by the diverging part of the interatomic potential $\phi(\boldsymbol{r})$ close to $\boldsymbol{r}$ = 0 and is positive up to large $\boldsymbol{q}$. However, the diverging part of $\phi(\boldsymbol{r})$ is never relevant because atoms do not come so close to each other. Therefore, we can remove the diverging part to define the pseudopotential as

$$\phi(r) = \phi_{pp}(r) + \phi_R(r) \tag{10}$$

where $\phi_{pp}(\boldsymbol{r})$ is the pseudopotential defined by $\phi_{pp}(r) = \phi(r_c)$ for $r < r_c$ and $\phi_{pp}(r) = \phi(r)$ for $r \geq r_c$ [45]. The cutoff distance, r_c, is chosen such that the cutoff temperature, $k_B T_u = \phi(r_c)$, is well above the actual temperature, and no pairs of atoms are found at distances of $r < r_c$. The potential energy has two parts,

$$U = U_{pp} + U_R, \tag{11}$$

where

$$U_{pp} = \int \rho(\boldsymbol{r})\rho^*(\boldsymbol{r}')\phi_{pp}(|\boldsymbol{r} - \boldsymbol{r}'|)d\boldsymbol{r}d\boldsymbol{r}', \tag{12}$$

$$U_R = \int \rho(\boldsymbol{r})\rho^*(\boldsymbol{r}')\phi_R(|\boldsymbol{r} - \boldsymbol{r}'|)d\boldsymbol{r}d\boldsymbol{r}'. \tag{13}$$

Because no pair of atoms are found within r_c, $U_R = 0$. Thus, we only need to evaluate U_{pp} to determine the structure, with the density wave theory in $\boldsymbol{q}$ space.

The Fourier-transform of the pseudopotential, $\phi_{pp}(\boldsymbol{q})$, was found to have a strong minimum close to the wavenumber expected for the DW state, $\boldsymbol{q_{DW}}$. Thus, we theorize that $\phi_{pp}(\boldsymbol{q})$ is driving the system to the DW state, resulting in the increase in ξ_s as the temperature is reduced [46,65,66]. However, the SRO of the DW state was found to be quite poor, with almost no icosahedral local structure [65]. Therefore, the DW state, obtained by minimizing the energy in $\boldsymbol{q}$ space, and the SRO, obtained by minimizing the energy in $\boldsymbol{r}$ space, are incompatible with each other. For this reason, the DW state cannot be reached even at $T = 0$. The value of T_{IG} in Equation (8) indicates the extent of this conflict. The ratio, T_{IG}/T_g, is related to liquid fragility [67]. Liquid fragility [28] is defined by

$$m = \left.\frac{dlog\eta(T)}{d(T_g/T)}\right|_{T_g} \tag{14}$$

where $\eta(T)$ is viscosity, and m describes how rapidly the viscosity changes near T_g. Liquids with larger values of m are called "fragile", whereas those with low m are called "strong". It reflects the degree of covalency of atomic bonds. Thus, T_{IG} increases with increased covalency.

In addition, local thermal fluctuations disrupt the long-range nature of the DW state. Such local thermal fluctuations can be described in terms of the atomic-level pressure or volume fluctuations. It can be shown [46] that

$$\frac{a}{\xi_s} = \frac{10\pi^3}{9}\left\langle \left(\varepsilon_V^R\right)^2 \right\rangle, \tag{15}$$

where a is the nearest neighbor distance. The local volume fluctuation, $\left\langle \left(\varepsilon_V^R\right)^2 \right\rangle$, has two components,

$$\left\langle \left(\varepsilon_V^R\right)^2 \right\rangle = \left\langle \left(\varepsilon_V^{R,mf}\right)^2 \right\rangle + \left\langle \left(\varepsilon_V^{R,th}\right)^2 \right\rangle, \tag{16}$$

where $\left\langle \left(\varepsilon_V^{R,mf}\right)^2 \right\rangle$ is the atomic-level misfit strain, and $\left\langle \left(\varepsilon_V^{R,th}\right)^2 \right\rangle$ is the thermal volume fluctuation. Because of the equipartition theorem for the atomic-level pressure fluctuations [68], the thermal volume fluctuation is given by

$$\left\langle \left(\varepsilon_V^{R,th}\right)^2 \right\rangle = \frac{(K_\alpha - 1)^2}{K_\alpha}\frac{k_B T}{2BV} \tag{17}$$

where B is bulk modulus, V is atomic volume, and K_α is the Eshelby parameter [69],

$$K_\alpha = \frac{3(1-\nu)}{2(1-2\nu)} \tag{18}$$

and ν is Poission's ratio. Therefore,

$$\frac{\xi_s}{a} = C\frac{T_g}{T - T_{IG}} \tag{19}$$

where

$$C = \frac{9}{10\pi^3}\frac{K_\alpha}{(K_\alpha - 1)^2}\frac{2BV}{k_B T_g} \tag{20}$$

$$T_{IG} = \frac{K_\alpha}{(K_\alpha - 1)^2}\frac{2BV}{k_B}\left\langle \left(\varepsilon_V^{R,mf}\right)^2 \right\rangle \tag{21}$$

The MRO, however, freezes at the glass transition. The glass transition temperature is given by

$$T_{IG} = \frac{2BV}{k_B K_\alpha} \left\langle \left(\varepsilon_V^{T,crit} \right)^2 \right\rangle \quad (22)$$

where $\varepsilon_V^{T,crit} = 0.095$ is the universal critical strain determined by the percolation of liquid-like atomic sites [47]. This theory describes the results of an experiment and simulation with high quantitative accuracy for metallic liquids and provides a reasonable explanation of other properties [46,66].

4. Dynamic Correlation in Superfluid ^{4}He

We now turn our focus to the atomic dynamics in ^{4}He, which becomes superfluid due to the Bose–Einstein (BE) condensation. The BE condensation is well-defined for an ideal gas, whereas He atoms interact through the Lennard–Jones potential. As a result, only about 7% of He atoms condense to the BE state [70]. Thus, the PDF of ^{4}He determined by neutron scattering which shows the average interatomic distance of 3.6 Å [71] describes essentially the structure of uncondensed atoms. To determine the structure of the BE condensed atoms, we measured the dynamic structure factor, $S(\boldsymbol{q}, E)$, of ^{4}He by inelastic neutron scattering and transformed it to the energy-resolved PDF, $g(\boldsymbol{r}, E)$ [48], defined by

$$g(r, E) = \frac{1}{N} \sum_{i,j} \int \delta\left(r - \left|\boldsymbol{r_i}(0) - \boldsymbol{r_j}(t)\right|\right) exp(i\omega t) dt, \quad (23)$$

where $\boldsymbol{r_i}(t)$ is the position of the i-th atom at time t and $E = \hbar\omega$.

The signature of the B–E condensate is the roton excitation, which has a sharp feature at 0.7 meV. So, if we focus on $g(\boldsymbol{r}, E)$ at 0.7 meV, we are primarily looking at condensed atoms. Particularly, by comparing $g(\boldsymbol{r}, E)$ above and below the BE condensation temperature, T_{BE}, we can extract the atomic correlations in the condensate. We discovered that the interatomic distance for the BE condensed atoms is 4 Å [48], much longer than that of the uncondensed atoms [71]. To illustrate this difference, we compare the total PDF (in red) against the integral of $g(\boldsymbol{r}, E)$ from E = 0.69 to 0.9 meV (in blue) in Figure 4. It is clear that upon BE condensation, the first peak shifts outward by 0.3 Å or more. We explained this difference in terms of atomic wavefunction overlap [49]. In the condensed state, the wavefunctions of different atoms cannot overlap, because it would lead to level-splitting. To achieve orthogonalization with spatially extended wavefunctions, the ground state has to be a macroscopic resonant state, just as in the resonant valence bond (RVB) state [72]. However, slow dynamics will not allow the system to reach such a massive resonant ground state, just as an antiferromagnet stays in the Néel state even though the true quantum ground state is the resonant singlet state [73]. The simplest alternative is to eliminate the wavefunction overlap by atoms becoming separated a little further. As a result, the interatomic distance is larger than in the uncondensed state where a small overlap is allowed, just as in the exchange hole compared to the correlation hole for electrons [74].

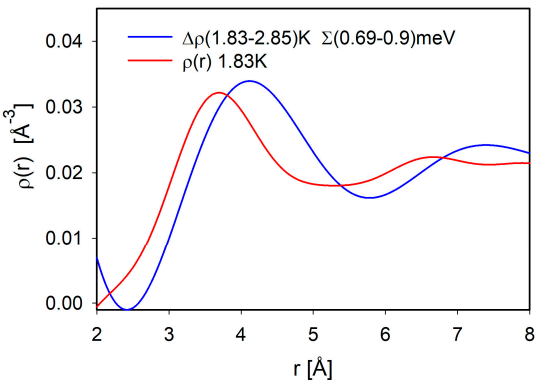

Figure 4. The total PDF (red) and the roton portion (0.69–0.9 meV) of the difference in the energy-resolved PDFs of ^{4}He, $\Delta g(r, E) = g_{T1}(r, E) - g_{T2}(r, E)$ (blue), for $T1$ = 1.83 K and $T2$ = 2.85 K [48].

5. Dynamic Correlation among Electrons

Our method to observe dynamic correlations in real space and time using the energy-resolved PDF [48] and the Van Hove function [75,76],

$$G(r,t) = \frac{1}{N}\sum_{i,j}\delta\left(r - \left|\boldsymbol{r_i}(0) - \boldsymbol{r_j}(\boldsymbol{t})\right|\right), \tag{24}$$

can be applied to electrons to observe dynamic correlations among electrons. For atoms, the classical interpretation of the correlation functions, Equations (1), (23) and (24), are valid, but for electrons, we have to be more careful about the quantum effect. The inelastic X-ray scattering cross-section of electrons is given by [77],

$$\frac{d\sigma}{d\omega d\Omega} = \sigma_0 S(q,\omega) = \frac{\sigma_0}{2\pi}\sum_{k.k'}\int\left\langle c_{\boldsymbol{k}}^{+}(t)c_{\boldsymbol{k}+\boldsymbol{q}}(t)c_{\boldsymbol{k}'+\boldsymbol{q}}^{+}(0)c_{\boldsymbol{k}'}(0)\right\rangle e^{-i\omega t}dt, \tag{25}$$

where $c_{\boldsymbol{k}}^{+}(t)$ creates a fermion with the momentum $\boldsymbol{k}$ at time t, $\sigma_0 = e^2/m$, e is the electron charge, m is the electron mass, and <. . .> denotes quantum and thermal average. Usually, the decoupling by the random-phase approximation (RPA),

$$\left\langle c_{\boldsymbol{k}}^{+}(t)c_{\boldsymbol{k}+\boldsymbol{q}}(t)c_{\boldsymbol{k}'+\boldsymbol{q}}^{+}(0)c_{\boldsymbol{k}'}(0)\right\rangle \rightarrow \left\langle c_{\boldsymbol{k}+\boldsymbol{q}}(t)c_{\boldsymbol{k}'+\boldsymbol{q}}^{+}(0)\right\rangle\left\langle c_{\boldsymbol{k}}^{+}(t)c_{\boldsymbol{k}'}(0)\right\rangle, \tag{26}$$

is applied, and

$$\left\langle c_{\boldsymbol{k}+\boldsymbol{q}}(t)c_{\boldsymbol{k}'+\boldsymbol{q}}^{+}(0)\right\rangle\left\langle c_{\boldsymbol{k}}^{+}(t)c_{\boldsymbol{k}'}(0)\right\rangle = \delta_{\boldsymbol{k},\boldsymbol{k}'}\left(1-n_{\boldsymbol{k}+\boldsymbol{q}}\right)n_{\boldsymbol{k}}\delta\left(\omega - \left(E_{\boldsymbol{k}+\boldsymbol{q}} - E_{\boldsymbol{k}}\right)/\hbar\right)e^{i\omega t} \tag{27}$$

where $n_{\boldsymbol{k}} = \left\langle c_{\boldsymbol{k}}^{+}c_{\boldsymbol{k}}\right\rangle$. Thus, the dynamic structure factor, $S(\boldsymbol{q}, \omega)$, describes the excitation of electrons from below the Fermi level to above it. It is also interpreted as the imaginary part of the dielectric response function [78].

However, the RPA decoupling in reciprocal space erases the phase relationship between the initial and final states in the transition, which contains the information on the real-space correlations. To avoid this loss of phase information and to observe the correlation in real space, we introduce a real-space description,

$$c_{\boldsymbol{k}}^{+}(t) = \int c^{+}\left(\boldsymbol{r}',t\right)e^{-i\boldsymbol{k}\cdot\boldsymbol{r}'}d\boldsymbol{r}', \quad c_{\boldsymbol{k}+\boldsymbol{q}}(t) = \int c(\boldsymbol{r}'',t)e^{i(\boldsymbol{k}+\boldsymbol{q})\cdot\boldsymbol{r}''}d\boldsymbol{r}''. \tag{28}$$

where $c^{+}(\boldsymbol{r},t)$ is a fermion creator at $\boldsymbol{r}$ and t. Then,

$$\begin{array}{c} c_{\boldsymbol{k}}^{+}(t)c_{\boldsymbol{k}+\boldsymbol{q}}(t)c_{\boldsymbol{k}'+\boldsymbol{q}}^{+}(0)c_{\boldsymbol{k}'}(0) = \int c^{+}(\boldsymbol{r}',t)c(\boldsymbol{r}'',t)c^{+}(\boldsymbol{r}''',0)c(\boldsymbol{r}'''',0)\times \\ exp\left(i\left[-\boldsymbol{k}\cdot\boldsymbol{r}' + (\boldsymbol{k}+\boldsymbol{q})\cdot\boldsymbol{r}'' - \left(\boldsymbol{k}'+\boldsymbol{q}\right)\cdot\boldsymbol{r}''' + \boldsymbol{k}'\cdot\boldsymbol{r}''''\right]\right)d\boldsymbol{r}'d\boldsymbol{r}''d\boldsymbol{r}'''d\boldsymbol{r}''''. \end{array} \tag{29}$$

The intermediate scattering function [79],

$$F(\boldsymbol{q},t) = \int S(q,\omega)e^{i\omega t}d\omega, \tag{30}$$

is given by

$$F(\boldsymbol{q},t) = \sum_{k'k'}\left\langle c_{\boldsymbol{k}}^{+}(t)c_{\boldsymbol{k}+\boldsymbol{q}}(t)c_{\boldsymbol{k}'+\boldsymbol{q}}^{+}(0)c_{\boldsymbol{k}'}(0)\right\rangle. \tag{31}$$

In the real-space representation, Equation (29), the summation over $\boldsymbol{k}$ and $\boldsymbol{k'}$ in Equation (31) yields $\boldsymbol{r'} = \boldsymbol{r''}$, $\boldsymbol{r'''} = \boldsymbol{r''''}$. Then,

$$\begin{array}{l} F(\boldsymbol{q},t) = \int\left\langle c^{+}(\boldsymbol{r}',t)c(\boldsymbol{r}',t)c^{+}(\boldsymbol{r}''',0)c(\boldsymbol{r}''',0)\right\rangle exp(i\boldsymbol{q}\cdot(\boldsymbol{r}'-\boldsymbol{r}'''))d\boldsymbol{r}'d\boldsymbol{r}''' \\ = \int\left\langle(\boldsymbol{r}',t)(\boldsymbol{r}''',0)\right\rangle exp(i\boldsymbol{q}\cdot(\boldsymbol{r}'-\boldsymbol{r}'''))d\boldsymbol{r}'d\boldsymbol{r}''', \end{array} \tag{32}$$

where

$$\rho(\boldsymbol{r},t) = c^{+}(\boldsymbol{r},t)c(\boldsymbol{r},t) \tag{33}$$

is the local density operator. Thus, the Van Hove function is expressed as the density correlation function in real space and time,

$$G(\boldsymbol{r},t) = \int F(\boldsymbol{q},t)e^{i\boldsymbol{q}\cdot\boldsymbol{r}}d\boldsymbol{q} = \int \langle \rho(\boldsymbol{r}+\boldsymbol{r}',t)\rho(\boldsymbol{r}',0)\rangle d\boldsymbol{r}'. \quad (34)$$

This proves that the classical interpretation of the double-Fourier-transformation of $S(\boldsymbol{q}, E)$ as the Van Hove correlation function is valid, even for electrons. The energy-resolved PDF is given by

$$g(r,\omega) = \frac{1}{2\pi}\int G(r,t)e^{-i\omega t}dt. \quad (35)$$

We measured the electronic $S(\boldsymbol{q}, E)$ for polycrystalline beryllium by inelastic X-ray scattering with the incident energy of 11.32 keV and energy resolution of 0.7 eV at the Beamline 27ID-B of the Advanced Photon Source of Argonne National Laboratory. The preliminary result [80] shows the exchange-correlation hole with the radius of about 2 Å. Surprisingly, at the plasmon energy of about 20 eV, the exchange-correlation hole is extended to about 5 Å. In a plasmon, electrons are dynamically correlated, resulting in larger separation among electrons than in electrons at large. This result demonstrates that the dynamic state of electrons affects electron correlations. The details of this observation will be reported elsewhere.

6. Implication on High-Temperature Superconductivity

The combination of the result on ^{4}He and the observation of electron correlations by inelastic X-ray scattering have very significant implications on the high-temperature superconductivity of the cuprates. In the regular BCS superconductors, electrons are in the Fermi-liquid state, and they are gas-like as discussed above. Electrons avoid each other by forming exchange-correlation holes, and the density functional theory (DFT) [81] works. The Cooper pairs are large, up to 1000 Å, and they strongly overlap with each other. If they are stable up to high temperatures, they would B-E condense at temperatures of the order of 1000 K. Thus, the pairing temperature determines the superconducting critical temperature, T_c.

In contrast, in the cuprates, electrons are strongly correlated, just as in supercooled liquids in which the potential energy is as important as the kinetic energy. For this reason, it is interesting to note that it was recently found that in the overdoped cuprates, the periodicity of the charge density wave was independent of the Fermi momentum as the doping density was changed [82]. It is likely that the Coulomb repulsion energy is involved in the formation of the density waves, for instance, through the pseudopotential discussed above [45,66].

Furthermore, in the cuprates, the Cooper pairs are small, of the order of nm in size, and low in density. Thus, they are likely to be preformed above the superconducting transition temperature [83–85]. If that is the case, T_c is equal to T_{BE}, and it is controlled by the BE condensation rather than by pairing. We speculate that as in the case of ^{4}He the separation between Cooper pairs is longer in the BE condensate than in the normal state to avoid wavefunction overlap. Then, the Coulomb repulsion energy is reduced in the BE condensate compared to the normal state, adding to the driving force for the BE condensation [49]. The difference is similar to the case of exchange and correlation effects for fermions, so the energy difference must be related to the exchange constant.

This effect is most likely negligible for ^{4}He, because the interaction energy (van der Waals force) is small. However, for the cuprates, a small change in the repulsion energy can have a very significant effect. Because the hole density is low, the energy associated with the wavefunction overlap is a small percentage of U. Nevertheless, the on-site Coulomb repulsion, U, is nearly 10 eV for Cu [74], which is huge in contrast to k_BT_c~10 meV. Although the value of U itself may not be influenced by the BE condensation, slight changes in the extent of the *p-d* hybridization due to the BE condensation can affect the total repulsion energy. Thus, a tiny change in the repulsion energy can have a major effect on T_c. It is

interesting to note that the pseudogap temperature, T^*, extrapolates to zero just beyond the optimum doping [86]. If T^* is the pair formation temperature, T_c should go down as well in the conventional pairing picture. It is possible that the repulsion energy reduction mechanism discussed here is maintaining the high value of T_c beyond the optimum doping. So far, the effort to increase T_c has focused on the pairing force. This new mechanism calls for a change in strategy, to increase T_c through the correlation effects.

To test this hypothesis, we plan to measure the $g(\boldsymbol{r}, E)$ for doped holes in the superconducting cuprates with inelastic X-ray scattering. The measurement is quite difficult because of the low intensity of the signal due to the high-energy resolution (better than 10 meV) required to observe the energy gap and due to the low doping density. However, this is within the realm of feasibility with advanced facilities.

7. Conclusions

Gases and liquids are fundamentally different in the role of the interatomic potentials. In gases, atomic interactions are collisional, and the average potential energy is negligibly small compared to the kinetic energy. In liquids, the potential energy is as important as the kinetic energy and results in complex atomic dynamics. An important consequence of the interatomic potential is the formation of the atomic medium-range order (MRO) which affects many properties. We propose a density wave theory to describe the behavior of the MRO. We suggest that this difference between gases and liquids can be instructive in discussing the difference in dynamics between nearly free electrons and strongly correlated electrons. We point out that electron correlation can be influenced by the dynamic state of electrons. In particular, the Bose–Einstein condensation of Cooper pairs could affect electron correlation energy, giving rise to an additional driving force to increase the superconducting transition temperature.

Funding: This work was supported by the U. S. Department of Energy, Office of Science, Basic Energy Sciences, Materials Science and Engineering Division.

Data Availability Statement: Data used in this work are available upon request from the corresponding author.

Acknowledgments: The author is grateful to Peter Fulde for his encouragement.

Conflicts of Interest: The author declares no conflicts of interest.

References

1. Landau, L.D.; Lifshitz, E.M. *Statistical Physics*; Sykes, J.B.; Kearsley, M.J., Translators; Addison-Wesley: Boston, MA, USA, 1958.
2. Egelstaff, P.A. *An Introduction to the Liquid State*, 2nd ed.; Oxford University Press: Oxford, UK, 1991.
3. Croxton, C.A. *Liquid State Physics—A Statistical Mechanical Introduction*; Cambridge University Press: Cambridge, MA, USA, 1974.
4. Hansen, J.-P.; McDonald, I.R. *Theory of Simple Liquids*, 2nd ed.; Academic Press: Cambridge, MA, USA, 2006.
5. Wallace, D.C. Statistical mechanics of monoatomic liquids. *Phys. Rev. E* **1997**, *56*, 4179–4186. [CrossRef]
6. Wallace, D.C. Liquid dynamics theory of high-temperature specific heat. *Phys. Rev. E* **1998**, *57*, 1717–1722. [CrossRef]
7. Kittel, C. *Introduction to Solid State Physics*; John Wiley & Sons: Hoboken, NJ, USA, 1953.
8. Egami, T. Understanding the Properties and Structure of Metallic Glasses at the Atomic Level. *J. Metals* **2010**, *62*, 70–75. [CrossRef]
9. Moon, J.; Lindsay, L.; Egami, T. Atomic dynamics in fluids: Normal mode analysis revisited. *Phys. Rev. E* **2023**, *108*, 014601. [CrossRef] [PubMed]
10. Ornstein, L.S.; Zernike, F. Accidental deviations of density and opalescence at the critical point of a single substance. *Roy. Neth. Acad. Arts Sci. (KNAW)* **1914**, *17*, 793–806.
11. Perkus, J.K.; Yevick, G.J. Analysis of classical statistical mechanics by means of collective coordinates. *Phys. Rev.* **1958**, *110*, 1–13. [CrossRef]
12. Bernal, J.D. A geometrical approach to the structure of liquids. *Nature* **1959**, *183*, 141–147. [CrossRef]
13. Bernal, J.D. Geometry of the structure of monatomic liquids. *Nature* **1960**, *185*, 68–70. [CrossRef]
14. Finny, J. Random packing and the structure of simple liquids. I. The geometry of random close packing. *Proc. Roy. Soc. Lond. A* **1970**, *319*, 479–493.
15. Cohen, M.H.; Turnbull, D. Molecular transport in liquids and glasses. *J. Chem. Phys.* **1959**, *31*, 1164–1169. [CrossRef]
16. Turnbull, D.; Cohen, M.H. Free-volume model of the amorphous phase: Glass transition. *J. Chem. Phys.* **1961**, *34*, 120–125. [CrossRef]

17. Turnbull, D.; Cohen, M.H. On the free-volume model of the liquid-glass transition. *J. Chem. Phys.* **1970**, *52*, 3038–3041. [CrossRef]
18. Mori, H. Transport, collective motion and Brownian motion. *Prog. Theor. Phys.* **1965**, *33*, 423. [CrossRef]
19. Kadanoff, L.; Swift, J. Transport coefficients near liquid-gas critical point. *Phys. Rev.* **1968**, *166*, 89–101. [CrossRef]
20. Kawasaki, K. Kinetic equations and time correlation functions of critical fluctuations. *Ann. Phys. N. Y.* **1970**, *61*, 1–56. [CrossRef]
21. Goldstein, M. Viscous liquids and the glass transition: A potential energy barrier picture. *J. Chem. Phys.* **1969**, *51*, 3728–3739. [CrossRef]
22. Stillinger, F.H. A topological view of supercooled liquids and glass formation. *Science* **1995**, *267*, 1935–1939. [CrossRef]
23. Wales, D.J. *Energy Landscapes*; Cambridge University Press: Cambridge, MA, USA, 2003.
24. Dyre, J.C.; Olsen, N.B.; Christensen, T. Local elastic expansion model for viscous-flow activation energies of glass-forming molecular liquids. *Phys. Rev. B* **1996**, *53*, 2171–2174. [CrossRef]
25. Leutheusser, E. Dynamical model of the liquid-glass transition. *Phys. Rev. A* **1984**, *29*, 2765–2773. [CrossRef]
26. Götze, W.; Sjogren, L. Relaxation processes in supercooled liquids. *Rep. Prog. Phys.* **1992**, *55*, 241–376.
27. Das, S.P. Mode-coupling theory and the glass transition in supercooled liquids. *Rev. Mod. Phys.* **2004**, *76*, 785–851. [CrossRef]
28. Angell, C.A. Formation of glasses from liquids and biopolymers. *Science* **1995**, *267*, 1924–1935. [CrossRef] [PubMed]
29. Debenedetti, P.G.; Stillinger, F.H. Supercooled liquids and the glass transition. *Nature* **2001**, *410*, 259–267. [CrossRef]
30. March, N.H.; Tosi, M.P. *Introduction to Liquid State Physics*; World Scientific: Singapore, 2002.
31. Faupel, F.; Macht, M.P.; Mehrer, H.; Naundorf, V.; Rätzke, K.; Schober, H.R.; Sharma, S.K.; Teichler, H. Diffusion in metallic glasses and supercooled melts. *Rev. Mod. Phys.* **2003**, *75*, 237–280. [CrossRef]
32. Scopigno, T.; Ruocco, G.; Sette, F. Microscopic dynamics in liquid metals: The experimental point of view. *Rev. Mod. Phys.* **2005**, *77*, 881–933. [CrossRef]
33. Dyre, J.C. The glass transition and elastic models of glass-forming liquids. *Rev. Mod. Phys.* **2006**, *78*, 953–972. [CrossRef]
34. Lubchenko, V.; Wolynes, P.G. Theory of structural glasses and supercooled liquids. *Ann. Rev. Phys. Chem.* **2007**, *58*, 235–266. [CrossRef]
35. Götze, W. *Complex Dynamics of Glass-Forming Liquids*; Oxford University Press: Oxford, UK, 2009.
36. Donth, E. *The Glass Transition: Relaxation Dynamics of Liquids and Disordered Materials*; Springer: Berlin, Germany, 2010.
37. Liu, A.J.; Nagel, S.R. The jamming transition and the marginally jammed solid. *Ann. Rev. Cond. Mat.* **2010**, *1*, 347–369. [CrossRef]
38. Parisi, G.; Zamponi, F. Mean-field theory of hard sphere glasses and jamming. *Rev. Mod. Phys.* **2010**, *82*, 789–845. [CrossRef]
39. Berthier, L.; Biroli, G. Theoretical perspective on the glass transition and amorphous materials. *Rev. Mod. Phys.* **2011**, *83*, 587–645. [CrossRef]
40. Edigar, M.D.; Harrowell, P. Perspective: Supercooled liquids and glasses. *J. Chem. Phys.* **2012**, *137*, 080901. [CrossRef]
41. Dyre, J.C. Perspective: Excess-entropy scaling. *J. Chem. Phys.* **2018**, *149*, 210901. [CrossRef] [PubMed]
42. Parisi, G.; Urbani, P.; Zamponi, F. *Theory of Simple Glasses: Exact Solutions in Infinite Dimensions*; Cambridge University Press: Cambridge, MA, USA, 2020.
43. Weeks, J.D.; Chandler, D.; Andersen, H.C. Role of repulsive forces in determining the equilibrium structure of simple liquids. *J. Chem. Phys.* **1971**, *54*, 5237–5247. [CrossRef]
44. Egami, T. Atomic level stresses. *Progr. Mater. Sci.* **2011**, *56*, 637–653. [CrossRef]
45. Egami, T.; Ryu, C.W. Structural principles in metallic liquids and glasses: Bottom-up or top-down. *Front. Mater.* **2022**, *9*, 874191. [CrossRef]
46. Egami, T.; Ryu, C.W. Medium-range atomic correlation in simple liquid. II. Theory of temperature dependence. *Phys. Rev. E* **2021**, *104*, 064110. [CrossRef] [PubMed]
47. Egami, T.; Poon, S.J.; Zhang, Z.; Keppens, V. Glass transition in metallic glasses: A microscopic model of topological fluctuations in the bonding network. *Phys. Rev. B* **2007**, *76*, 024203. [CrossRef]
48. Dmowski, W.; Diallo, S.O.; Lokshin, K.; Ehlers, G.; Ferré, G.; Boronat, J.; Egami, T. Observation of dynamic atom-atom correlation in liquid helium in real space. *Nat. Commun.* **2017**, *8*, 15294. [CrossRef]
49. Egami, T.K. Alex Müller and superconductivity. *Physica C* **2023**, *613*, 1354345. [CrossRef]
50. Frank, F.C. Supercooling of liquids. *Proc. Roy. Soc. Lond. A* **1952**, *215*, 43–46.
51. Turnbull, D. Kinetics of solidification of supercooled liquid mercury droplets. *J. Chem. Phys.* **1952**, *20*, 411–424. [CrossRef]
52. Sadoc, J.F. Use of regular polytopes for the mathematical description of the order in amorphous structures. *J. Non-Cryst. Solids* **1981**, *44*, 17–30. [CrossRef]
53. Sethna, J.P. Frustration and curvature: Glasses and the cholesteric blue phase. *Phys. Rev. Lett.* **1983**, *51*, 2198–2201. [CrossRef]
54. Nelson, D.R. Order, frustration, and defects in liquids and glasses. *Phys. Rev. B* **1983**, *28*, 5515–5535. [CrossRef]
55. Steinhardt, P.J.; Nelson, D.R.; Ronchetti, M. Icosahedral bond order in supercooled liquids. *Phys. Rev. Lett.* **1981**, *47*, 1297–1300. [CrossRef]
56. Tomida, T.; Egami, T. Molecular-dynamics study of orientational order in liquids and glasses and its relation to the glass transition. *Phys. Rev. B* **1995**, *52*, 3290–3308. [CrossRef] [PubMed]
57. Miracle, D.B. A structural model for metallic glasses. *Nat. Mater.* **2004**, *3*, 697–702. [CrossRef]
58. Sheng, H.W.; Luo, W.K.; Alamgir, F.M.; Bai, J.M.; Ma, E. Atomic packing and short-to-medium-range order in metallic glasses. *Nature* **2006**, *439*, 419–425. [CrossRef]
59. Warren, B.E. *X-ray Diffraction*; Addison-Wesley, Reading: Boston, MA, USA, 1969.

60. Egami, T. Local Density Correlations in Liquids. *Front. Phys.* **2020**, *8*, 50. [CrossRef]
61. Zhou, Y.; Mei, B.; Schweizer, K.S. Integral equation theory of thermodynamics, pair structure, and growing static length scale in metastable hard sphere and Weeks-Chandler-Andersen fluids. *Phys. Rev. E* **2020**, *101*, 042121. [CrossRef]
62. Kleban, P. Toward a microscopic basis for the de Gennes narrowing. *J. Stat. Phys.* **1974**, *11*, 317–322. [CrossRef]
63. Cargill, G.S., III. Structure of metallic alloy glasses. *Solid State Phys.* **1975**, *30*, 227–320.
64. Ryu, C.W.; Dmowski, W.; Egami, T. Ideality of liquid structure: A case study for metallic alloy liquids. *Phys. Rev. E* **2020**, *101*, 030601(R). [CrossRef] [PubMed]
65. Ryu, C.W.; Dmowski, W.; Kelton, K.F.; Lee, G.W.; Park, E.S.; Morris, J.R.; Egami, T. Curie-Weiss behavior of liquid structure and ideal glass state. *Sci. Rep.* **2019**, *9*, 18579. [CrossRef]
66. Egami, T.; Ryu, C.W. Origin of medium-range atomic correlation in simple liquid: Density wave theory. *AIP Adv.* **2023**, *13*, 085308. [CrossRef]
67. Ryu, C.W.; Egami, T. Origin of liquid fragility. *Phys. Rev. E* **2020**, *102*, 042615. [CrossRef] [PubMed]
68. Levashov, V.A.; Aga, R.S.; Morris, J.R.; Egami, T. Equipartition theorem and the dynamics of liquids. *Phys. Rev. B* **2008**, *78*, 064205. [CrossRef]
69. Eshelby, J.D. The determination of the elastic field of an ellipsoidal inclusion, and related problems. *Proc. Roy. Soc. Lond. A* **1957**, *241*, 376–396.
70. Glyde, H.R. *Excitations in Liquid and Solid Helium*; Clarendon Press: Oxford, UK, 1994.
71. Svensson, E.C.; Sears, V.F.; Woods, A.D.B.; Martel, P. Neutron-diffraction study of the static structure factor and pair correlations in liquid ^{4}He. *Phys. Rev. B* **1980**, *21*, 3538–3651. [CrossRef]
72. Anderson, P.W. The resonating valence bond state in La_2CuO_4 and superconductivity. *Science* **1987**, *235*, 1196–1198. [CrossRef]
73. Keffer, F. *Spin waves, in Handbuch Der Physik, 18, pt. 2*; Springer: Berlin, Germany, 1966.
74. Fulde, P. *Electron Correlations in Molecules and Solids*; Springer: Berlin, Germany, 2012.
75. Van Hove, L. Correlation in space and time and Born approximation scattering in systems of interacting particles. *Phys. Rev.* **1954**, *95*, 249–262. [CrossRef]
76. Egami, T.; Shinohara, Y. Perspective: Correlated atomic dynamics in liquid seen in real space and time. *J. Chem. Phys.* **2020**, *153*, 180902. [CrossRef] [PubMed]
77. Platzman, P.M.; Tzor, N. X-ray scattering from electron gas. *Phys. Rev.* **1965**, *139*, A410–A413. [CrossRef]
78. Abbamonte, P.; Finkelstein, K.D.; Collins, M.D.; Gruner, S.M. Imaging density disturbances in water with a 41.3-attosecond time resolution. *Phys. Rev. Lett.* **2004**, *92*, 237401. [CrossRef] [PubMed]
79. Lovesey, S.W. *Theory of Neutron Scattering from Condensed Matter*; Oxford University Press: Oxford, UK, 1984.
80. Bista, R.; Upton, M.; Shinohara, Y.; Egami, T. Direct observation of electron correlation in space by inelastic x-ray scattering. 2024; *unpublished*.
81. Kohn, W.; Sham, L.J. Self-consistent equations including exchange and correlation effects. *Phys. Rev.* **1965**, *140*, A1133–A1138. [CrossRef]
82. Li, Q.; Huang, H.-Y.; Ren, T.; Weschke, E.; Ju, L.; Zou, C.; Zhang, S.; Qiu, Q.; Liu, J.; Ding, S.; et al. Prevailing charge order in overdoped $La_{2-x}Sr_xCuO_4$ beyond the superconducting dome. *Phys. Rev. Lett.* **2023**, *131*, 116002. [CrossRef]
83. Emery, V.J.; Kivelson, S.A. Importance of phase fluctuations in superconductors with small superfluid density. *Nature* **1995**, *374*, 434–437. [CrossRef]
84. Uemura, Y.J. Bose-Einstein to BCS crossover picture for high-T_c cuprates. *Phys. C* **1997**, *282–287*, 194–197. [CrossRef]
85. Xu, Z.A.; Ong, N.P.; Wnag, Y.; Kakeshita, T.; Uchida, S. Vortex-like excitations and the onset of superconducting phase fluctuation in underdoped $La_{2-x}Sr_xCuO_4$. *Nature* **2000**, *406*, 486–488. [CrossRef]
86. Tallon, J.L.; Lorum, J.W. The doping dependence of T*—What is the real Tc phase diagram? *Phys. C* **2001**, *349*, 53–68. [CrossRef]